Straining to Learn Permeability

Bryan Euser [1], Christopher W. Johnson[1], Robert A. Guyer [1,2], Esteban Rougier [1], Carly M. Donahue [1], George Guthrie [1], Antonio Munjiza [3], Paul A. Johnson [1]

[1]Los Alamos National Laboratory
[2]University of Nevada, Reno
[3]FGAG, University of Split, Split, Croatia

Key Points:

- Fluid flow simulations through a channel are examined to identify elastic fingerprints of fluid flow characteristics
- We find equations of state relating strain and acoustic emission to permeability using measurements made outside the porous material
- Flow-induced noise, or acoustic emissions, may ultimately describe fluid mobility characteristics with remote measurements

Corresponding author: Bryan Euser, `beuser@lanl.gov`

Abstract

Characterizing fluid flow in a porous material with permeability is fundamental to energy and hydrological applications, yet direct measurements of permeability are very difficult to conduct *in situ*. However, attending fluid flow through a material are various mechanical responses, e.g., strain fields, acoustic emission. These mechanical responses may hold important clues to the fluid flow in the material, to the permeability. Here we report results from a numerical study of fluid flow in a channel, defined by confining side blocks, that contains a particle bed. For a range of inlet velocities, we study the strain and acoustic emission in the side blocks. Simulations are repeated for different configurations of the particle bed. We find that the observed mechanical response accords with an analytic model of this system, providing promising evidence for using mechanical measurements, particularly strain and acoustic emission, as surrogates for direct measurement of permeability.

Plain Language Summary

Formation permeability is an important quantity to know for energy reservoirs as well as for aquifers and faulted regions; however, permeability is challenging to measure in Earth. We have devised an approach based on numerical simulations of fluid flow in a channel that contains particles, where the strain field is detected and used to measure channel permeability. We also find that characteristics of the acoustic emission from the flow channel can be used to determine the permeability.

1 Introduction

What is being suggested by "straining to learn permeability" is that remote mechanical measurements of a fluid through porous material may contain descriptive information to quantify properties of the fluid flow through the material. A porous material is characterized by the porosity, ϕ, a measure of how much pore space is in the material, and the permeability, k, a measure of how much fluid flows through the material in response to a pressure gradient. It is conventional to describe the components in measurement of fluid flow with Darcy's law,

$$\frac{Q}{A} = -\frac{k}{\mu}\nabla P, \tag{1}$$

where μ is the viscosity of the fluid in the pore space of the material in steady state, Q is the quantity of fluid flowing through cross-section A of the material, and ∇P is the pressure gradient across the material. The permeability, k, is the transport coefficient that relates the driving force, ∇P, to the current, Q, the analogue of Ohm's law $I = (1/R)V$, $(1/R) \rightarrow k$. The permeability is a global quantity, belonging to a material, not to a point in the material. Direct measurement of k requires two measurements, of pressure to find ∇P, and measurement of the fluid flow Q (the same at all points in the material in steady state). Such measurements are difficult to carry out *in situ*, and most are made on cores studied in a lab or from modeling the permeability using auxiliary measurements provided by various well logs.

Our interest is in possible mechanical schemes to get at the permeability. Prompted in part by recent success in using acoustic emission to follow the time evolution of stick-slip mechanical systems, e.g., (Rouet-Leduc et al., 2017, 2018, 2020; P. A. Johnson et al., 2021; Lubbers et al., 2018; Hulbert et al., 2020; C. W. Johnson & Johnson, 2021; Wang et al., 2021), we are now examining the use of mechanical measurements to quantify properties of a fluid-carrying channel. The first component of this examination is the numerical study that we present here. We introduce a numerical model of a fluid-carrying channel that contains a particle bed through which the fluid must flow. To give proper treatment of the solid component of the system, the fluid component of the system, and the solid-fluid coupling we use the Hybrid Optimization Software Suite (HOSS; Knight et al., 2020) computational

scheme that has proved valuable in handling complex fluid-solid systems. We introduce this computational scheme in Sec. 2. In Sec. 3 we describe our findings using a strain field measured in the side blocks adjacent to the flow channel and the acoustic emission measured in the side blocks adjacent to the flow channel. We find that the pressure and strain field obey behavior suggested by a theory of the fluid flow (Appendix I) and that these quantities can be related to the measured permeability.

2 Materials and methods

We undertake a D=2 numerical simulation of fluid flow through a particle bed confined to a segment of a channel (Figure 1). The solid component of this system contains two side blocks that define a channel with a particle bed. Water flows through the system. The system is studied using HOSS, a finite-discrete element method (FDEM) code; FDEM combines aspects of the finite element method (FEM) and the discrete element method (DEM). The FDEM was originally developed for simulating failure processes in brittle materials. It has since been used to model a wide variety of complex physical systems, e.g., earthquake rupture, high-strain-rate impact (Okubo et al., 2019; Froment et al., 2020). Here, FEM treatment is given to the interior elastic structure of the two side blocks and the interior elastic structure of the particles. The encounters between particle-particle and particle-side block engage the DEM component of FDEM. The equation governing the displacement $\mathbf{x}$ of a node in the solid component of the system is

$$\mathbf{M}\frac{d^2\mathbf{x}}{dt^2} + \mathbf{C}\frac{d\mathbf{x}}{dt} + \mathbf{K}\mathbf{x} = \mathbf{f}, \tag{2}$$

where **M, C, K** are the mass matrix, damping matrix, and stiffness matrix, respectively, and $\mathbf{f}$ is the force on the node. HOSS supports a fluid-solid interaction solver (Munjiza et al., 2020). This allows a fluid component of the system, a Navier-Stokes fluid that sees the solid component, to be followed with the conservation laws for mass, energy, and momentum. The fluid exists on an Eulerian grid that lies atop the Lagrangian FDEM grid. The basic fluid-solid interaction originates with the fluid adjacent to solid moving with the motion of the solid. This interaction is implemented using a closed-form immersed boundary method (Peskin, 1972). The physical parameters characterizing the solid and the fluid are exhibited in Fig. 1. The solid body mesh has an average element size of 15 μm and the fluid mesh is a rectangular grid of 5 μm cells. A second-order central difference time integration scheme is used to obtain the temporal evolution of the system (Munjiza & Rougier, 2010; Munjiza et al., 2011).

2.1 Computational Model

The system, length 3960 μm and width 3300 μm, comprises two side blocks with elastic properties of granite, with width 1100 μm bounding a channel of width 1100 μm. In the center of the channel, realizations of 60 particles of diameter 100 μm are arranged randomly with approximate porosity of 40%. These particle arrangements are not stable two dimensional particle arrangements, i.e., 60 particles cannot hold themselves stably in such a configuration. A mechanical superstructure is introduced that holds adjacent particles near one another and holds the particle assembly locally in the channel. The fluid does not interact with this superstructure. The superstructure allows the fluid forces acting on the particles to be transmitted throughout the particle bed and to be delivered to the side blocks (Figure 1).

The model design allows us to emulate a D=3 fluid-solid system in a D=2 framework. To limit the motion of the side blocks to motion caused only by fluid flow through the particle bed, we introduce a small gap between the fluid and solid phase that separates the solid blocks from the fluid. Therefore, the sole elastic coupling from the fluid/particle bed configuration is via the particle bed superstructure. The three outer edges of the side blocks

that do that not make up the fluid channel are assigned boundary conditions that restrict all translational and rotational motion. In the fluid domain, a constant inlet velocity is imposed on the far left and a constant outlet pressure (P= 0) is imposed on the far right. There are "sensors" placed throughout the solid material, that collect the particle displacement, velocity, etc. point-wise in the solid. The simulations were run for a 4000 μs duration. A typical simulation takes about 20 hrs of computation time on 72 processors to complete. Results from four realizations of the 60 particle bed are described.

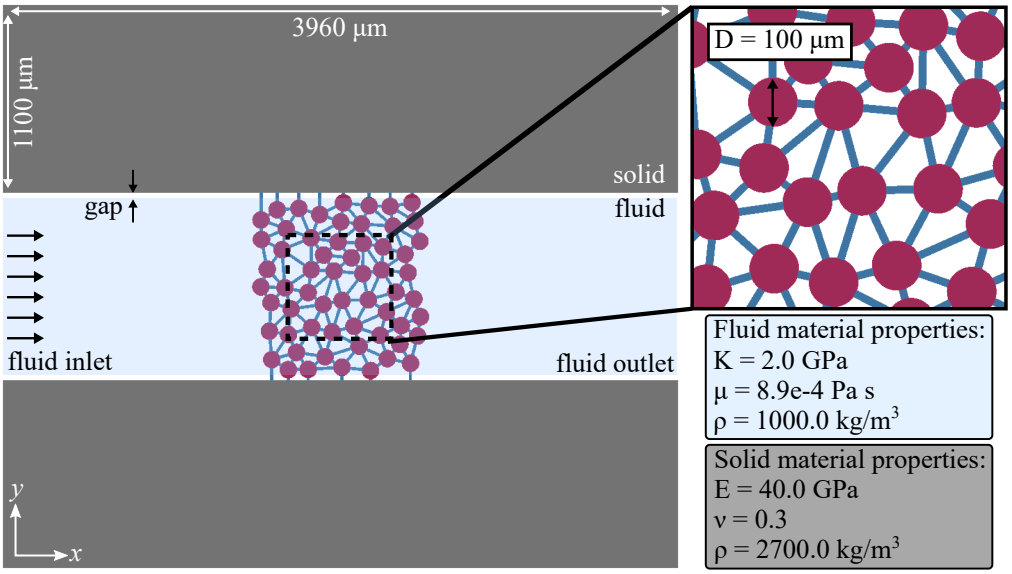

Figure 1. Schematic of the numerical model. A channel, defined by two side blocks, contains a particle bed. Flow from $-x$ to $+x$ is through the particle bed. The particles are elastically coupled to each other and the side blocks via a mechanical superstructure that does not impede fluid flow (see inset showing expanded view of mechanical superstructure and particle bed). The two insets at bottom right lists the material properties.

3 Results and Discussion

The simulation system is examined at constant current, i.e., steady state. We set the inlet velocity, U (0.5 m/sec $< U <$ 3.75 m/sec), and the outlet pressure (P = 0.0 for all U). The system is allowed to come to a steady (current carrying) state after which various outputs are recorded. An illustration of the behavior of the fluid in steady state is shown in Figure 2 as $U(\mathbf{x},t) = |(U_x(\mathbf{x},t), U_y(\mathbf{x},t)|$ with the inlet velocity U set to 2.0 m/sec. As a consequence, an average pressure drop, P, of approximately 2×10^5 Pa is set-up between the inlet and outlet. We make a judgement about when steady state is reached by monitoring the fluctuations in this average pressure drop. Steady state quantities are extracted during the last 1000 μsec of a run, i.e., over a time domain of length T. While the spatial pattern of fluid velocity, $U(\mathbf{x},t)$, throughout the system is of interest, we turn attention to three measures of the consequence of the fluid flow. In the steady state time domain we record two "quasi-static" measures of the response as (1) the inlet pressure in the fluid, P, and (2) the a strain, ϵ, in the side blocks (adjacent to the fluid channel). Additionally, in this time domain, we record the mechanical fluctuations (the acoustic emission) in the side blocks (Figure 2).

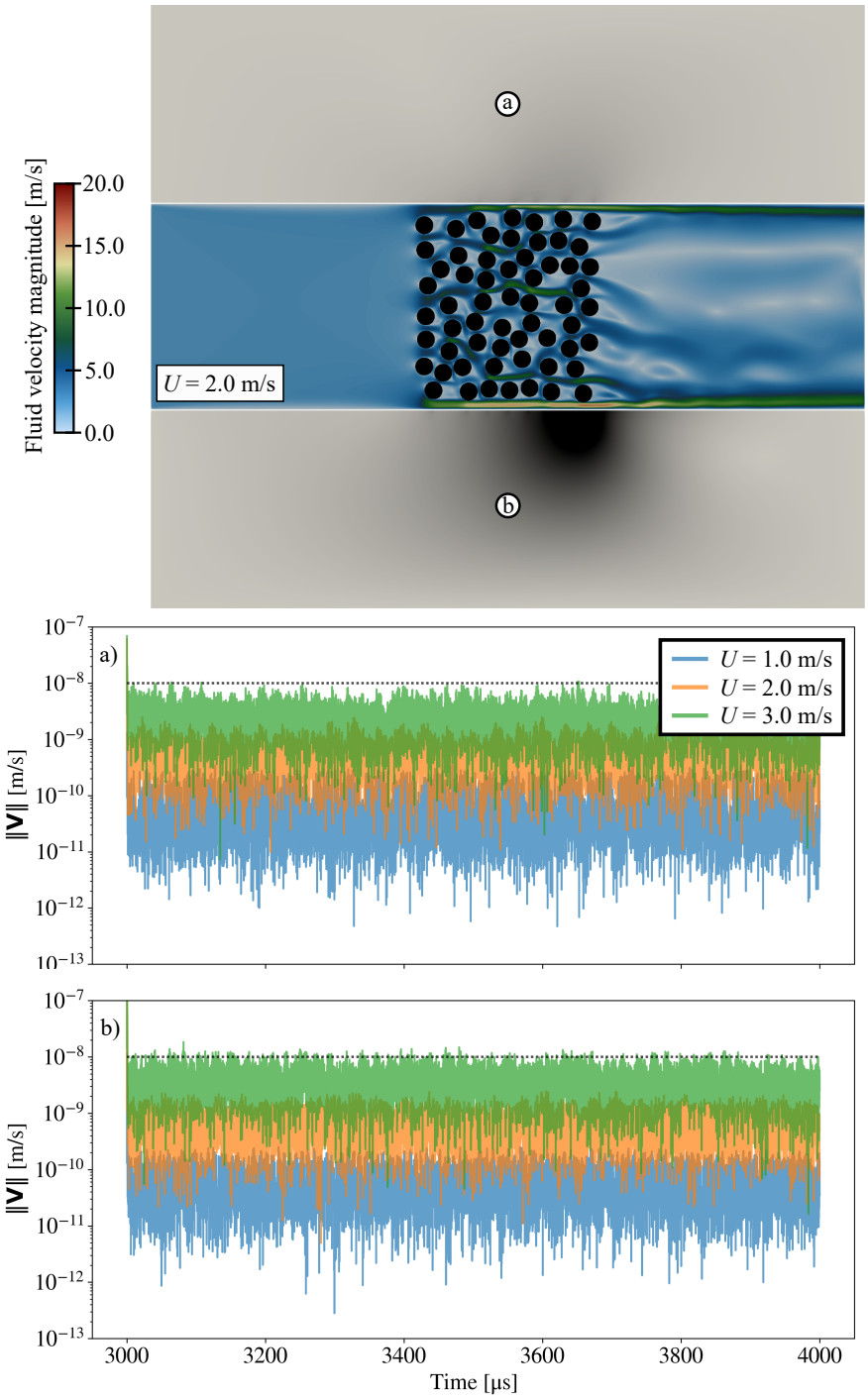

Figure 2. Fluid/solid velocities. (a) For the case inlet velocity $v_{\text{inlet}} = 2.0$ m/s at time $t = 4000$ μs the fluid velocity is plotted, see color scale. In the domain of the side blocks a gray scale shows the amplitude of the acoustic emission. (b) and (c) The magnitude of the acoustic emission received at two points in the side blocks during the steady state time domain. As explained in the text acoustic emission is associated with the fluctuation of the velocity of points in the side blocks. The dotted black line acts as a reference between the data shown in (b) and (c).

3.1 Quasi-static response

In Figure 3a we show the inlet-outlet pressure difference, P, as a function of inlet velocity (0.5 m/sec $< U <$ 3.75 m/sec) for 4 realizations of the particle bed. In Figure 3b we show the strain $\epsilon = \partial u_x/\partial y$ in the side block (adjacent to the fluid) as a function of the inlet velocity for 4 realizations of the particle bed. Both P and ϵ scale as U^2. These results are in accord with the model for the forces in the system described in the Appendix and they are not trivial.

1. The proportionality of P and ϵ to U^2 establishes that the Reynolds number characterizing the flow is $\gg 1$. It is the fluid motion in the pore space that sets the Reynolds number, not some *a priori* assessment of the fluid motion. That is, the Reynolds number characterizing the fluid motion results from the experience the fluid has as it traverses the system.
2. There are two *equations of state* for the quasi-static variables describing the system; see Appendix. These are
$$P = \chi_P \, U^2, \quad \epsilon = \chi_\epsilon \, U^2, \tag{3}$$
where χ_P and χ_ϵ are constants related to the geometrical structure of the pore space. These equations can be manipulated to give
$$k^{-1} \propto \frac{P}{U} = \frac{\chi_p}{\sqrt{\chi_\epsilon}}\sqrt{\epsilon}, \tag{4}$$
where k is the permeability. In principle, a measurement of the strain gives the permeability. What is crucial to the use of this equation is having the means to learn the constants that turn proportionality into equivalence.

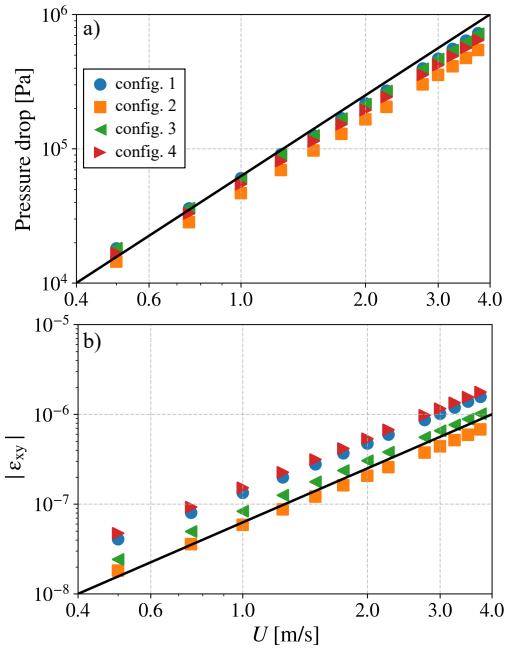

Figure 3. Quasi-static measured quantities. (a) Pressure drop across the system as a function of inlet velocity for 4 realizations of the particle bed. (b) Strain in the upper side block as a function of inlet velocity for 4 realizations of the particle bed. The scale is *log-log* so that the slope 2 is easily illustrated.

3.2 Dynamic response.

At each sensor location $\mathbf{x}_i$ in the side blocks we form

$$\overline{V}(\mathbf{x}_i) = \frac{1}{T}\int_T V(\mathbf{x}_i, t)\ dt, \quad \textit{and} \quad \delta V^2(\mathbf{x}_i) = \frac{1}{T}\int_T \left[V(\mathbf{x}_i, t) - \overline{V}(\mathbf{x}_i)\right]^2\ dt, \tag{5}$$

where $V = |(V_x, V_y)|$, $\overline{V}(\mathbf{x}_i)$ is the average of $V(\mathbf{x}_i, t)$ over time T and $\delta V(\mathbf{x}_i)$ is a measure of the fluctuations in the velocity at $\mathbf{x}_i$. For $\mathbf{x}_i$ at the midpoints of the side blocks we show $V(\mathbf{x}_i, t)$ over the steady state time domain T in Figure 2a and 2b.

We examine the connection between the velocity fluctuations in the side blocks and the permeability. For each U we have

$$k(U) = \mu L\ \frac{U}{\Delta P(U)}\ , \tag{6}$$

where $L = 3960$ μm and μ is the viscosity of the fluid. For each U this permeability is averaged over the 4 realizations of the particle bed to form $\langle k(U)\rangle$. Similarly, for each U we average $\delta V(\mathbf{x}_{mid})$ over the 4 realizations of the particle bed to form $\langle \delta V(U)\rangle$. We illustrate the connection between these realization averaged quantities in Figure 4 where we show $\langle k(U)\rangle$ as a function of $\langle \delta V(U)\rangle$. The one-to-one relationship between $\langle k(U)\rangle$ and $\langle \delta V(U)\rangle$ constitutes an empirical equation of state which, in principle, allows one to determine the permeability of the particle bed from a measurement of the amplitude of the velocity fluctuations in the domain (side blocks) adjacent to the particle bed. We do not have a phenomenology, like that for the quasi-static response (Appendix I), for the connection between $\langle k(U)\rangle$ and the fluid motions that are responsible for the fluctuations $\delta V(\mathbf{x}_i)$ and $\langle \delta V(U)\rangle$. Models applying machine learning are in development to map the connection between permeability and particle velocity in the side blocks into a generalized framework that predicts the permeability directly from the acoustic emission noise, or flow-induced weak vibrations. Additionally, porous media fluid-flow experiments to further elucidate/validate the numerical simulations and provide laboratory support for these findings is in progress.

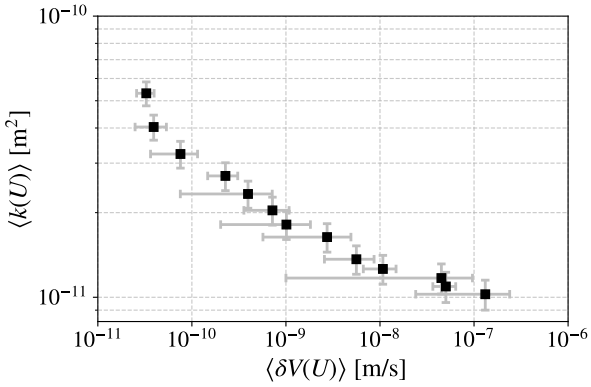

Figure 4. Dynamic measurements. Realization average permeability as a function of the realization average of δV, i.e., for each U, k and δV are from the average over 4 realizations of the particle bed.

4 Conclusion

We have constructed a D=2 model of flow through porous material in a channel, defined by two side blocks, that we examine employing the HOSS computational scheme. We

study this model when it is carrying a constant fluid current. We measure the pressure difference necessary to maintain the current and obtain permeability of the porous material by conventional methods. We focus on the examination of the mechanical response of the side blocks in which the porous material resides. We measure two types of mechanical response: (1) quasi-static, the strain field developed in the side blocks, and (2) dynamic, the acoustic emission measured in the side blocks. The results show that the strain measured in the side blocks is related to the pressure drop in the porous material and that the acoustic emission, measured as the particle velocity in the side blocks, is a sensitive function of the current in the porous material. Thus, these remote elastic measurements, i.e., in the side blocks, contain information broadcast from the fluid-flow with which one can learn the permeability.

Acknowledgments

BE and CD acknowledge partial support from the Department of Energy (DOE) SMART Initiative. PAJ, CWJ, RAG, ER, and BE acknowledge support from the U.S. Department of Energy, Office of Science, Office of Basic Energy Sciences, Chemical Sciences, Geosciences, and Biosciences Division under grant 89233218CNA000001. We thank the LANL Institutional Computing program for their support in generating data used in this work. This work has been approved for unlimited release by LANL under LA-UR-22-21129.

References

Froment, M., Rougier, E., Larmat, C., Lei, Z., Euser, B., Kedar, S., ... Lognonné, P. (2020). Lagrangian-based Simulations of Hypervelocity Impact Experiments on Mars Regolith Proxy. *Geophysical Research Letters*, *47*(13), 1–8. doi: 10.1029/2020GL087393

Hulbert, C., Rouet-Leduc, B., Jolivet, R., & Johnson, P. A. (2020). An exponential build-up in seismic energy suggests a months-long nucleation of slow slip in cascadia. *Nature Communications*, *11*(1), 4139. doi: 10.1038/s41467-020-17754-9

Johnson, C. W., & Johnson, P. A. (2021). Learning the low frequency earthquake daily intensity on the central san andreas fault. *Geophysical Research Letters*, *48*(15), e2021GL092951. doi: 10.1029/2021GL092951

Johnson, P. A., Rouet-Leduc, B., Pyrak-Nolte, L. J., Beroza, G. C., Marone, C. J., Hulbert, C., ... Reade, W. (2021). Laboratory earthquake forecasting: A machine learning competition. *Proceedings of the National Academy of Sciences*, *118*(5). doi: 10.1073/pnas.2011362118

Knight, E. E., Rougier, E., Lei, Z., Euser, B., Chau, V., Boyce, S. H., ... Froment, M. (2020). HOSS: an implementation of the combined finite-discrete element method. *Computational Particle Mechanics*, *7*(5), 765–787. doi: 10.1007/s40571-020-00349-y

Lubbers, N., Bolton, D., Mohd-Yusof, J., Marone, C., Barros, K., & Johnson, P. (2018). Earthquake catalog-based machine learning identification of laboratory fault states and the effects of magnitude of completeness. *Geophysical Research Letters*, *45*. doi: 10.1029/2018GL079712

Munjiza, A., Knight, E. E., & Rougier, E. (2011). *Computational Mechanics of Discontinua*. doi: 10.1002/9781119971160

Munjiza, A., & Rougier, E. (2010). MRCK_3D contact detection algorithm. In *Proceedings of the fifth international conference on discrete element methods* (pp. 37–45). London.

Munjiza, A., Rougier, E., Lei, Z., & Knight, E. E. (2020). FSIS: a novel fluid–solid interaction solver for fracturing and fragmenting solids. *Computational Particle Mechanics*. doi: 10.1007/s40571-020-00314-9

Okubo, K., Bhat, H. S., Rougier, E., Marty, S., Schubnel, A., Lei, Z., ... Klinger, Y. (2019). Dynamics, Radiation, and Overall Energy Budget of Earthquake Rupture With Coseismic Off-Fault Damage. *Journal of Geophysical Research: Solid Earth*, *124*(11), 11771–11801. doi: 10.1029/2019JB017304

Peskin, C. S. (1972). Flow patterns around heart valves: A numerical method. *Journal of*

Computational Physics, *10*(2), 252-271. doi: 10.1016/0021-9991(72)90065-4

Rouet-Leduc, B., Hulbert, C., Bolton, D. C., Ren, C. X., Riviere, J., Marone, C., ... Johnson, P. A. (2018). Estimating fault friction from seismic signals in the laboratory. *Geophysical Research Letters*, *45*(3), 1321–1329. doi: 10.1002/2017GL076708

Rouet-Leduc, B., Hulbert, C., Lubbers, N., Barros, K., Humphreys, C. J., & Johnson, P. A. (2017). Machine learning predicts laboratory earthquakes. *Geophysical Research Letters*, *44*(18), 9276–9282. doi: 10.1002/2017GL074677

Rouet-Leduc, B., Hulbert, C., McBrearty, I. W., & Johnson, P. A. (2020). Probing slow earthquakes with deep learning. *Geophysical Research Letters*, *47*(4), e2019GL085870. doi: 10.1029/2019GL085870

Wang, K., Johnson, C. W., Bennett, K., & Johnson, P. A. (2021, 12). Predicting fault slip via transfer learning. *Nature Communications*, *12*. doi: 10.1038/s41467-021-27553-5

Appendix A Phenomenology for quasi-static behavior of channel-particle bed model

A cartoon of the model for the fluid carrying pore space is shown in Fig. A1. The model is in D=2. Two side blocks define a channel that is filled with fluid. A particle bed resides in the channel. The particle arrangements of the particle bed are not natural D=2 arrangements. They are formed with a mechanical superstructure that holds the particles in relative position with sensible forces. As it moves through the channel the fluid sees the particles in the particle bed but it does not see the superstructure. The superstructure is anchored in the side blocks. The fluid, moving through the particle bed drags the particle bed to the right. The mechanical superstructure, anchored in the side blocks, attempts to hold the particle bed in place with forces that shear the side blocks. We look at the mechanical behavior of the side blocks (strain, displacement and velocity fluctuations, etc.) to get at what is happening in the fluid-particle bed system. Key ingredients in the model system are the microscopic lengths (a, b). For a suitably large simulation the spectrum of these lengths characterizes a pore space comprising a square (cubic) lattice of micro-channels, radius a and length b. The particle bed is the material volume in which this plumbing system resides.

The model system is studied in steady current states: (1) the fluid velocity is made uniform on the left, U, Fig. 1 in text, and (2) the pressure is made constant on the right at $P = 0$, Fig. 1 in text. Of interest at constant current state U are the pressure required to maintain the current, the forces on the fluid, the forces on the particle bed, and the forces on the side blocks. As this is an analytic study it is carried out in D=3.

A1 Constant current

When the system is in steady state there is a constant quantity of fluid crossing every cross-section of the system. A plane perpendicular to the x axis contains $\pi R^2/b^2$ pieces, micro-channel + particle bed. Each micro-channel oriented along x carries the amount of fluid $q = \pi a^2 V$, where V is the velocity of the fluid in the micro-channel having radius a. Thus

$$Q = \pi R^2 U = \frac{\pi R^2}{b^2} q = \frac{\pi R^2}{b^2} \pi a^2 V. \tag{A1}$$

Then $V = \frac{b^2}{\pi a^2} U \gg U$ for $b \gg a$.

A2 Forces

We assess the force on the fluid from the pressure, the force between the fluid and the particle bed, and the force between the particle bed and the side blocks.

1. The total force on the fluid due to the pressure is

$$F_{P\to F} = \frac{\pi R^2}{b^2}\pi a^2(P\ -\ 0) \tag{A2}$$

where P is the pressure on the left.

2. The total force from the fluid on the particle bed. The fluid momentum in a micro-channel arises from the pressure difference across the micro-channel, ΔP. This pressure difference applies the force $\Delta F = \pi a^2 \Delta P$ to the fluid for the time Δt giving rise to the momentum $\Delta(MV) = \rho\pi a^2 bV$ in the fluid in the channel

$$\Delta F \times \Delta t = \Delta(MV). \tag{A3}$$

There are two limits to consider, high and low V.

(a) Low fluid velocity (diffusion). The fluid in the micro-channel loses momentum to the walls of the micro-channel by a diffusion process in time $\Delta t = a^2/D_\mu$, where $\rho D_\mu = \mu$. Thus

$$\Delta P\pi a^2 \frac{a^2}{D_\mu} = \rho\pi a^2 bV \ \rightarrow\ \frac{\Delta P}{b}\frac{a^2}{\mu} = V. \tag{A4}$$

Each micro-channel obeys a local Darcy's law.

(b) High fluid velocity (translation). The fluid in the micro-channel loses momentum on the time scale for the fluid to traverse the micro-channel (i.e., the diffusion process is slow) $\Delta t = b/V$. Then

$$\Delta P\pi a^2 \frac{b}{V} = \rho\pi a^2 bV \ \rightarrow\ \frac{\Delta P}{\rho} = V^2. \tag{A5}$$

Each micro-channel has a pressure drop proportional to V^2.

(c) The Reynolds number, R_e. The Reynolds number is the ratio of the two times associated with the mechanisms of momentum loss, diffusion and translation. Form the Reynolds number

$$R_e = \frac{\Delta t_D}{\Delta t_T} = \frac{a^2/D_\mu}{b/V} = \frac{\mathcal{L}V}{D_\mu}, \tag{A6}$$

where $\mathcal{L} = a^2/b$ is a length. The numerical work in the text corresponds to $P \propto U^2$, Fig. 3. From here forward we use the $R_e \gg 1$ form of Δt.

The total force of the fluid on the particle bed is

$$F_{F\to pb} = N_3\frac{\Delta(MV)}{\Delta t} = N_3\frac{\rho\pi a^2 bV}{b/V} = N_3\rho\pi a^2 V^2, \tag{A7}$$

where $N_3 = \pi R^2 L/b^3$; $|F_{F\to pb}| = |F_{pb\to F}|$.

3. The force of the particle bed on the side blocks in which the channel is embedded is

$$F_{pb\to B} = G\epsilon \times 2\pi RL, \tag{A8}$$

where ϵ is the strain in the side blocks and G is the shear modulus of the side-blocks; $|F_{pb\to B}| = |F_{B\to pb}|$.

A3 Force balance

We have expressions for the forces between the system elements, fluid, particle bed, and side-blocks. Neither the fluid or side blocks are accelerated. Thus we have $F_{P\to F} + F_{pb\to F} = 0$ and $F_{F\to pb} + F_{B\to pb} = 0$.

1. There is no net force on the fluid.

$$F_{P\to F} = F_{bp\to F}, \quad \frac{\pi R^2}{b^2}\pi a^2 P = N_3 \rho \pi a^2 V^2, \tag{A9}$$

Replacing V by U from current conservation, Eq. (1), find

$$\frac{\pi R^2}{b^2}\pi a^2 P = N_3 \rho \pi a^2 \left(\frac{b^2}{\pi a^2}U\right)^2, \tag{A10}$$

or

$$\frac{P}{L} = \frac{b^3}{\pi^2 a^4}\ \rho U^2. \tag{A11}$$

2. There is no net force on the particle bed.

$$F_{F\to pb} = F_{B\to pb}, \quad N_3 \rho \pi a^2 V^2 = 2G\epsilon 2\pi RL. \tag{A12}$$

Replacing V by U from current conservation, Eq. (1), find

$$N_3 \rho \pi a^2 \left(\frac{b^2}{\pi a^2}U\right)^2 = 2G\epsilon 2\pi RL \tag{A13}$$

or

$$G\epsilon = \frac{bR}{4\pi a^2}\ \rho U^2. \tag{A14}$$

3. Results. The key results are in Eqs. (11) and (14)

$$\frac{P}{L} = \frac{b^3}{\pi^2 a^4}\ \rho U^2 \quad \to \quad P = \chi_P\ \rho U^2, \quad \chi_P = \frac{Lb^3}{\pi^2 a^4}, \tag{A15}$$

$$G\epsilon = \frac{bR}{4\pi a^2}\ \rho U^2 \quad \to \quad G\epsilon = \chi_\epsilon\ \rho U^2, \quad \chi_\epsilon = \frac{bR}{4\pi a^2}. \tag{A16}$$

These results are used in the text.

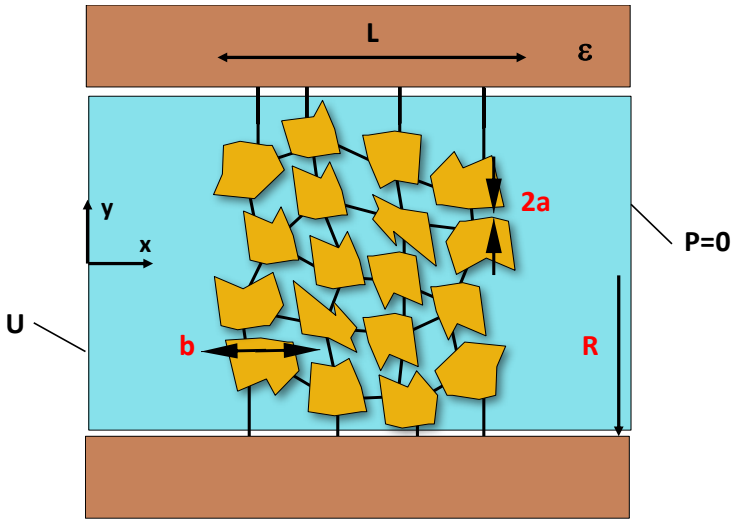

Figure A1. Cartoon of system. The 3 elements of the system are the fluid, the particle bed, and the side blocks. There are 4 lengths involved (R, L) macroscopic or channel scale and (a, b) microscopic or micro-channel scale. The steady current state corresponds to setting U on the left and $P = 0$ on the right.